Construction and Building Materials 289 (2021) 123046

Contents lists available at ScienceDirect

Construction and Building Materials

journal homepage: www.elsevier.com/locate/conbuildmat

The role of the hold-down in the capacity model of LTF and CLT shear walls based on the experimental lateral response

Angelo Aloisio [a], Francesco Boggian [b], Roberto Tomasi [c,*], Massimo Fragiacomo [a]

[a] Department of Civil, Construction-Architectural and Environmental Engineering, Università degli Studi dell'Aquila, L'Aquila, Italy
[b] Department of Civil, Environmental and Mechanical Engineering, University of Trento, Trento, Italy
[c] Faculty of Science and Technology, Norwegian University of Life Sciences, Ås, Norway

HIGHLIGHTS

- Pseudo-static cyclic tests on Cross-Lam Timber (CLT) and Light Timber Frame (LTF) shear walls.
- Decomposition of the post-elastic displacement into sliding, rocking and deformation components.
- Similarity of the two structural responses due to the same resisting mechanism.
- A capacity model based on the sole hold-down reaction seizes the overall cyclic response.
- The estimated overstrength factors manifests the intrinsic differences between the two structural systems.

ARTICLE INFO

Article history:
Received 6 October 2020
Received in revised form 8 March 2021
Accepted 10 March 2021
Available online 30 April 2021

Keywords:
Experimental cyclic response
Timber engineering
Shear walls
Rocking
Cross Laminated Timber
Light Timber Frame

ABSTRACT

Cross Laminated Timber (CLT) and Light Timber Frame (LTF) shear walls are widespread constructive technologies in timber engineering. Despite the intrinsic differences, the lateral response of the two structural systems may be quite similar under specific connection layouts, boundary constraints, and size of the shear walls. This paper compares the experimental cyclic responses of CLT and LTF shear walls characterized by the same size 250×250cm, and loaded according to the EN 12512 protocol. The rigid-body rotation of the shear walls prevails over the deformation and rigid-body translation in the post-elastic displacement range. As a consequence, a capacity model of the two systems based on the sole hold-down response accurately seizes the observed cyclic response, despite ignoring the other resisting contributions. The authors examine the differences exhibited by the CLT and LTF shear walls and the related error corresponding to a capacity model based on the sole hold down restraints. Additionally, it is assessed the overstrength of the CLT panel and LTF sheathing to the shear walls collapse due to the hold-down failure. The estimated overstrength factor is the most meaningful difference between the two structural systems in the considered experimental layouts.

1. Introduction

The use of timber in structural engineering is diverse across the centuries [1,2] and between geographical areas [3]. Currently, the most diffuse timber constructive systems in Europe are based on the use of Light Timber Frame (LTF) and Cross Laminated Timber (CLT) shear walls. LTF walls are made by a pinned-frame braced by OSB (Oriented Strand Board) or GFP (Gypsum Fiber Panel) sheathing panels, whereas CLT walls are solid-timber panels composed by layers of timber planks glued together [4,5]. The boost to the use of engineered wood products and timber engineering *tout court* stems from multiple reasons, e.g. the growing dominance of green engineering, and the economic and structural benefits in using timber products [6]. Additionally, the spreading of timber technologies in seismic-prone areas fed copious research activities devoted to the assessment of the lateral response of LTF and CLT structural systems via numerical and experimental investigations [7–9].

Many scholars attempt to develop structural systems alternative to the standard CLT and LTF shear walls by coupling dissipation devices [10,11], tuned mass dampers [12], and structural components which enhance ductility [13–15]. Most of the research pointed at developing predictive capacity models likely useful to

* Corresponding author.
E-mail addresses: angelo.aloisio1@univaq.it (A. Aloisio), francesco.boggian@unitn.it (F. Boggian), roberto.tomasi@nmbu.no (R. Tomasi), massimo.fragiacomo@univaq.it (M. Fragiacomo).

https://doi.org/10.1016/j.conbuildmat.2021.123046
0950-0618/

calibrate simplified design methods [16]. Predictive capacity models require experimental data for a proper calibration: numerous experimental campaigns evaluated the lateral responses of the two systems following distinct loading protocols and under diverse structural configurations [17–23].

The capacity model may gather in two main groups: those based on Finite Element (F.E.) and structural analysis [24–29], and empirical models [30–33]. The former ones strive to follow the experimental data and could be used in extrapolating the response of structural configurations different from those used for calibration. Conversely, empirical hysteresis models consist of algebraic or differential equations, which follow the experimental data, with no concern of the mechanical meaning of the employed parameters. These models cannot be used in extrapolating structural behaviours beyond those associated with the experimental data. However, the so-called empirical models are less time consuming than F.E. models and can be used to perform simulations in a relatively short time. Di Gangi et al. recently [34] reviewed the modeling strategies of timber shear walls from 1978 to 2018.

There are numerous and diverse capacity models in the scientific literature. Some researches merely attempt to elaborate closed-form models which best seize the observed response. Others, like [35], append to the mentioned efforts, an interpretative framework useful in developing simplified and reliable tools for the prediction of the lateral response. Specifically, [35] developed an analytical procedure and a simplified numerical model for the elastic response of LTF and CLT shear walls. They found that, in the elastic response range of CLT shear walls, 77% of the total displacement is due to rigid-body rotation, 16% to the rigid-body translation and 7% to the panel deformation. Conversely, in LTF shear walls, 45% is expected to the rigid-body rotation, 6% to the rigid body translation, and 45% and 4% to the sheathing-to-framing connection and sheathing panel deformation, respectively.

In this paper, the authors investigate CLT and LTF systems in the post-elastic range. The rigor and straightforwardness of elastic analysis vanishes when dissipative phenomena arise. The authors devoted their efforts in interpreting experimental data by clustering the displacement response in rocking, sliding and deformation components. In a second step, based on the observed results, an elementary capacity model based on the sole hold-down experimental response is compared to the experimental results to estimate the related approximation. The closeness between the experimental data of CLT and LTF shear walls inspire a conclusive remark about the disguised difference between them: the overstrength of the panel to the hold-downs. The different overstrength of the CLT and LTF panels is the actual feature which best distinguishes the natures of the two structural systems.

The first two sections describe the experimental cyclic tests of LTF and CLT shear walls, respectively. The third section analyses the displacement response by decomposing the rocking, sliding and deformation fractions. The fourth and fifth sections estimate the equivalent elastic stiffness in the elastic response range and the approximation in using a hold-down based capacity model. The last part addresses the differences between the two systems in term of overstrength.

2. Experimental cyclic tests of LTF and CLT shear walls

The results presented in this paper descend from the experimental data on LTF and CLT shear wall tests performed at the University of Trento. [36] have partially published the outcomes on LTF shear walls, while very limited results on CLT were published in [37–39]. The first part of this paper focuses on the description of the test setup and the experimental responses. The second part attempts to understand the leading deformation contributes to the shear walls lateral response and proposes a capacity model based on the hold-down contribution. The research novelty of this paper, with respect to [36,37], derives from the (1) complete report of the cyclic test results on CLT shear walls, (2) comparing CLT and LTF by decomposing the experimental response into rocking, sliding and deformation fractions, (3) the proposal of a novel capacity model driven by hold-down reactions, and (4) the estimation of overstrength factors.

The full description of the test setup of LTF and CLT shear walls is detailed in [40,41]. In this section, the authors will limit to a short description of the tested shear walls and features of the setup.

LTF shear walls with dimensions of 2.5×2.5 m were tested. The test set-up, shown in Fig. 1, follows the EN 594:2011 protocol [42]. Various vertical loads and different types of hold-downs, angle brackets and sheathing, drove a comparative assessment about the performance of the specimens. The LTF shear walls have the following characteristics: the frame elements are C24, with sec-

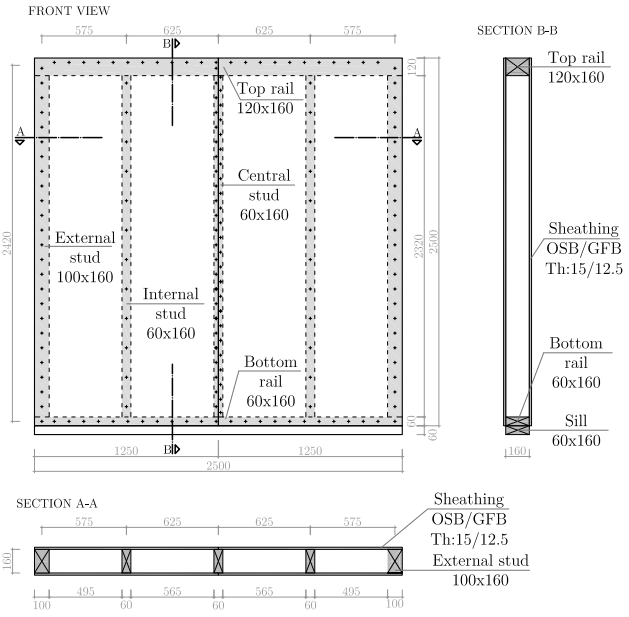

(a)

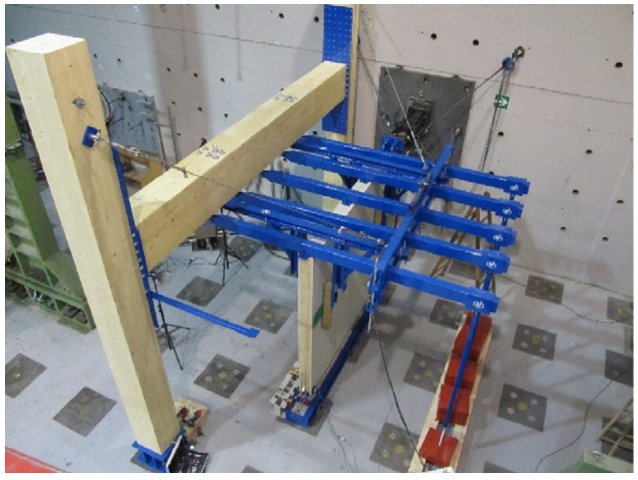

(b)

Fig. 1. (a) LTF specimen (measures in mm); (b) LTF test setup.

tions reported in Fig. 1. There are two types of sheathing: OSB/3 and GFP, with nails or staples as fasteners. The spacing of the sheathing-to-framing fasteners on the perimeter is also varied, and the spacing in the inner stubs always doubles the spacing of the perimeter, as shown in Table 1. Angle brackets or inclined screws resist against the shear wall sliding. Two types of hold-downs were tested, in addition to a specimen without any. The specimens labels follow this nomenclature: "LTF/CLT label-L number", where the label refers to the configuration explained in Table 1 and L identifies the vertical load in kN.

Table 2 summaries the primary outcomes of the cyclic tests. Table 2 reports only F_u and v_u, F_u measuring the strength capacity, while v_u the displacement capacity. The former expresses ultimate resistance; the latter is related to ductility. The optimum performance of a structural system derives from the optimum balance between resistance and ductility. Therefore, F_u and v_u may be suitable synthetic indicators of the experimental structural performance. Fig. 2 presents the results in the form of force–displacement curves.

The CLT shear walls have the following characteristics: three layers (thickness 30-30-30 mm) of C24 boards. Different vertical loads, various connections to the ground headed a comparative assessment between the specimens: precisely, three types of angle brackets, two types of hold-down and a specimen without hold-down-Table 2 reports the preliminary results of the cyclic tests. Fig. 4 depicts the force–displacement curves of the tested specimens. see Fig. 3. Table 3.

The experimental data deserve several and special considerations about the effect of the different connection layouts, vertical load, stiffness of the panel or the frame. Nevertheless, several research papers comment on this sort of results [7,36,28,19], and a mere comparative analysis between specimens would not add significant information to what is already published or acknowledged by the scientific community.

Still, the authors would comment on the analogies between the performances exhibited by the LTF and CLT shear walls. Table 2 attempts to compare the two structural typologies: in many specimens, the force and displacement data are quite similar. Averagely, the resistance of the CLT is higher than the LTF, whereas the ultimate displacement of the LTF is higher than the CLT. The crude conclusion is that the CLT and LTF shear walls exhibit an analogous behaviour, although the CLT system has a lower ductility than LTF.

The differences and analogies between the two classes of specimens may depend on the fact that the panel is adequately rigid to transfer the horizontal forces to the hold-downs. In particular, the discrepancies may depend on the different panel rigidity and the analogies on the use of the same connection layouts. The CLT and LTF shear wall in-plane stiffness determines a predominant rigid rocking, which causes the failure of the hold-downs. Accordingly, the entire panel testing is likely a test on its hold down connections, subjected to asymmetric cyclic loading. Therefore, the cyclic test of LTF and CLT shear walls would reduce to a sort of pull-out test of the hold-downs, since the wall assemblies behave like a rigid lever that transfers the load.

The validation of this hypothesis entails the assessment of the different contributions to the total displacement in the post-elastic range: rigid-body rotation, rigid-body translation and panel deformation. In this paper, the wall deformation encompasses all sorts of deformation related to the connection elements and the panel itself, namely: the nail slip between the sheathing (OSB, plywood, gypsum, plasterboard) and the timber frame, the shear distortion of the sheathing or the panel, the flexural deformation of the frame, and the slip of the wall relative to its base due to the flexibility of the hold-down and shear base connections.

3. Decomposition of the experimental cyclic response

The horizontal displacement of a shear wall may originate by summing the contributions of deformations from three primary sources: the rigid-body translation (sliding) and rotation (rocking), and the panel deformation (which includes all the contribution not included in the previous ones, such as sheathing-to-framing deformation for LTF and OSB/CLT in plane shear deformation). Differently from the elastic range, the influence of the three contributions changes with the load and the history of displacement. Still, it is attempted to derive the three parts which averagely comprise the total displacement at higher deformation.

The authors assume that the displacement measured in point D, Fig. 5(a), is representative of the sliding component. The deformation component arises from the relative displacement measured along the diagonals, while the rocking component arises from the vertical and horizontal displacements measured in C and B, respectively. The comparison between the sliding, rocking and deformation contributions of the considered shear walls will drive the

Table 1
Characteristics of the tested LTF shear walls.

Specimen LTF	STD	2F	150	50/RG	50	SCREW	WHD
Sheathing	OSB/3	GFB	OSB/3	OSB/3	OSB/3	OSB/3	OSB/3
Thickness [mm]	15	12.5	15	15	15	15	15
Fastener type	Ring nails	Staples	Ring nails	Ring nails	Ring nails	Ring nails	Ring nails
∅ [mm]	2.8	1.4x1.6	2.8	2.8	2.8	2.8	2.8
l [mm]	60	55	60	60	60	60	60
Perimerer spacing [mm]	100	100	150	50	50	100	100
Sliding restraint	New150	New150	New150	New150	New150	HBS	New150
n°	4	4	4	4	4	/	4
Fastener type	Anker nails	Anker nails	Anker nails	Anker nails	Anker nails	Screws	Anker nails
n°	12	12	12	12	12	25	12
∅ [mm]	4	4	4	4	4	8	4
l [mm]	60	60	60	60	60	180	60
Uplift restraint	WHT340	WHT340	WHT340	WHT620	WHT340	WHT340	/
n°	2	2	2	2	2	2	/
Fastener type	Anker nails	Anker nails	Anker nails	Anker nails	Anker nails	Anker nails	/
n°	20	20	20	52	20	20	/
∅ [mm]	4	4	4	4	4	4	/
l [mm]	60	60	60	60	60	60	/

Table 2
Cyclic test results: F_u, ultimate experimental racking load; v_u, slip corresponding to the ultimate load; both evaluated according to EN12512.

LTF			CLT		
Test	F_u [kN]	v_u [mm]	**Test**	F_u [kN]	v_u [mm]
STD-L0	47.6	60.6	STD-L0	55.6	42.2
STD-L10	58.1	78.4	STD-L20	80.2	43.3
STD-L20	57.5	74.5	NA620-L0	124.0	29.1
2F-L20	38.9	33.5	NA620-L20	146.5	28.6
150-L20	49.6	70.8	ND620-L0	132.9	30.4
50/RG-L20	97.6	76.0	ND620-L20	160.5	32.6
50-L20	65.5	53.5	NA340-L20	83.6	57.4
SCREW-L20	57.6	74.9	NAWH-L20	66.6	57.7
WHD-L10	34.0	54.1			

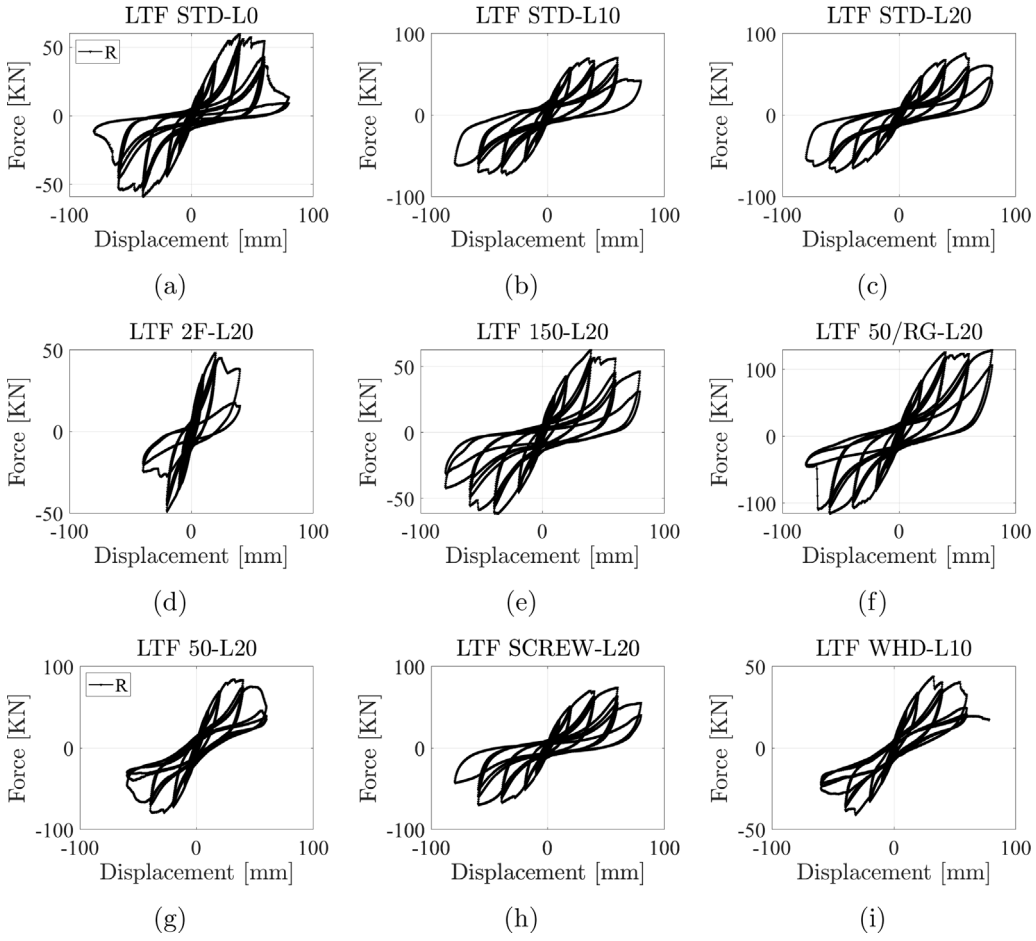

Fig. 2. Cyclic test results of LTF shear walls.

assessment of the approximation associated with an elementary capacity model.

3.1. Sliding

The sliding fraction is estimated as the limit of the ratio between the horizontal displacements in points D and B, as illustrated in Fig. 5(a):

$$s := \lim_{u_B \to \infty} \left| \frac{u_D(t)}{u_B(t)} \right| \quad (1)$$

The values of $u_D(t)$ and $u_B(t)$ are direct measures from the experimental campaign, and when plotted, they reveal an hyperbolic behaviour, with a clearly visible asymptote for higher values of the imposed displacement as seen in Fig. 5(c). The ratio in Eq. 1 is illustrated in a sample case by Figs. 5(c)-(d). At a lower displacement, the ratio tends to infinity: this is due to the division with almost zero displacement values imposed in B, while u_D may rest approximately constant at a low value. At higher displacement, the fraction tends towards two horizontal asymptotes. The main comments about Figs. 5(c)-(d) follow:

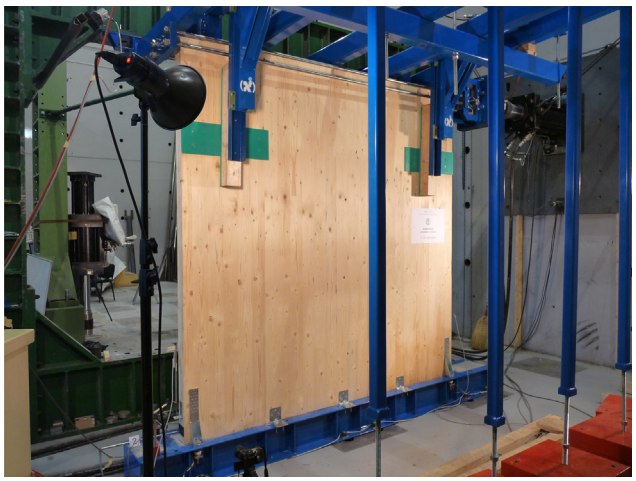

Fig. 3. CLT test setup.

- The ratios between the displacement measured in D and that imposed in B likely gather into beams of hyperbolae. In this case, it is focused on the first quadrant. The hyperbolae in the other quadrants derive from the combination of negative or positive components (Fig. 5(b)). Fig. 5(b) manifests that the displacements are not always concordant due to the "dragging" related to hysteresis phenomena.
- The higher is the imposed displacement, the higher is the sliding fraction. The horizontal asymptote of the beams of hyperbolae is non-negative, and it is likely a property of the test configuration, almost independent from the displacement value after a certain load level; The asymptote evidences the linear proportion between displacement in B and D at higher displacement values (Fig. 5(d)). The asymptote can be rightfully assumed as the sliding fraction of the imposed displacement.
- The curve followed in approaching the asymptote depends on the number of cycles. The arrow indicates the direction: the higher the cycle, the more the curve moves towards the upper right part of the quadrant. It possibly depends on the following evidence: a sliding fraction inherited by the previous cycle rises the u_D/u_B values when there are lower displacement values. The higher the cycle, the higher is the sliding fraction originated from the previous cycles: the growing plasticization of the shear wall components raises the fraction of permanent deformation on the total displacement.

3.2. Panel deformation

The relative displacement between the points A-C and B-D is a measure of the diagonal deformations in the East and West directions identified by d_E and d_W respectively. At this stage, the authors assume that the panel manifests a predominant shear deformation.

$$d_{E,W} = r_2 - r_1 \tag{2}$$

The shear displacement δ derives from Eq. 2 by expliciting the two radii r_2 and r_1, see Fig. 6(a):

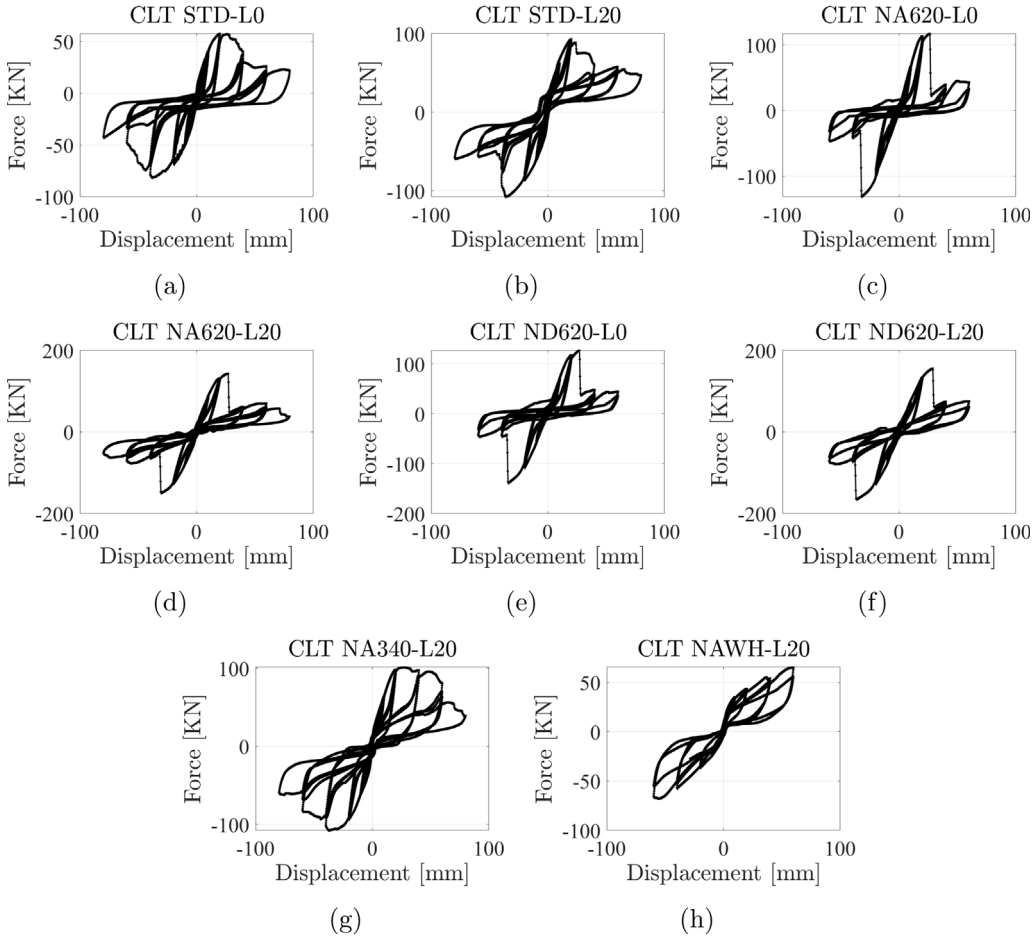

Fig. 4. Cyclic test results of CLT shear walls.

Table 3
Characteristics of the tested CLT shear walls.

Specimen CLT	STD	NA620	ND620	NA340	NAWH
Sliding restraint	100CR	10060newA	10060newD	10060newA	10060newA
n°	3	3	3	3	3
Fastener type	Anker nails	Anker nails	Anker nails	Anker nails	Anker nails
n°	12	30	30	30	30
∅ [mm]	4	4	4	4	4
l [mm]	60	60	60	60	60
Uplift restraint	WHT340	WHT620	WHT620	WHT340	/
n°	2	2	2	2	/
Fastener type	Anker nails	Anker nails	Anker nails	Anker nails	/
n°	20	52	52	20	/
∅ [mm]	4	4	4	4	/
l [mm]	60	60	60	60	/

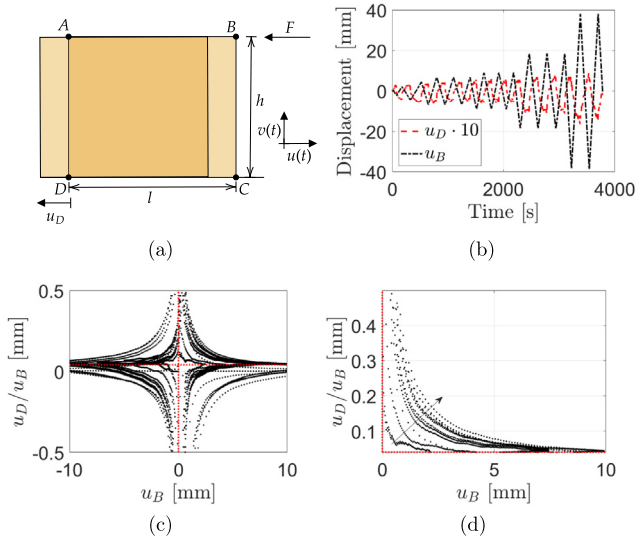

Fig. 5. (a) Illustration of the rigid-body translation of the panel and the adopted notation; (b) superposition between the displacements in B and D; (c)-(d) ratio between the displacement in D and B as a function of the imposed displacement according to the loading protocol.

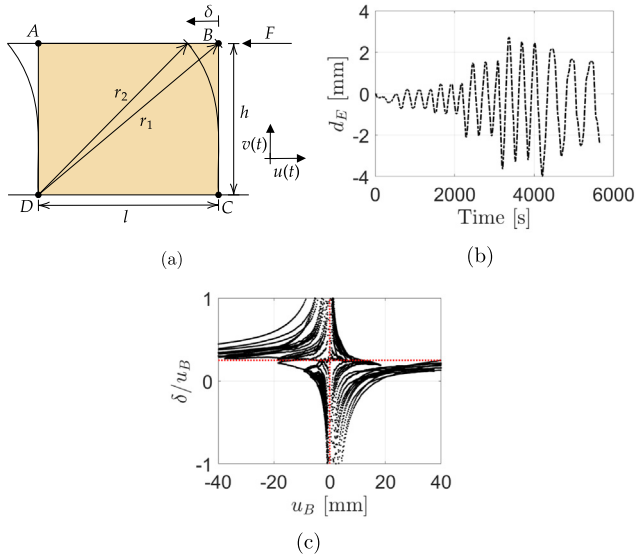

Fig. 6. (a) Illustration of the shear deformation of the panel and the adopted notation; (b) displacement-time curve of a sample diagonal relative displacement δ; (c) ratio between δ and u_B as a function of the imposed displacement according to the loading protocol.

$$\delta = l - \left[\left(h\sqrt{2} - d_{E,W}\right)^2 - h^2\right]^{0.5} \tag{3}$$

The ratio between δ and u_B approaches a constant value at higher displacement values. The following definition of the deformation fraction, d, attempts to grasp the approaching asymptot.

$$\mathrm{d} := \lim_{u_B \to \infty} \left|\frac{\delta}{u_B}\right| \tag{4}$$

At a lower displacement, the ratio tends to infinity: this is due to the division with almost zero displacement values imposed in B, while δ maintains a small plastic deformation which never approaches zero. The main comments about Fig. 6 follow:

- The sample relative displacement in Fig. 6(b) shows that the panel deformation almost follows the loading protocol, except for the last three cycles. At that stage, localized plastic deformations occur due to timber compression, and the definition in Eq. 4 may lose its accuracy.
- The ratio between δ and u_B tends to a constant value, although the beams of hyperbolae are not symmetric, as explained in the previous paragraphs, see Fig. 6(c).

3.3. Rocking

The rocking component is estimated as a complement to one of the already estimated sliding and deformation contributions:

$$r = 1 - (s + d) \tag{5}$$

The whole displacement field of the shear wall is illustrated in Fig. 7, where all the contribution to the top displacement u_B are highlighted: u_D represents the sliding contribution while δ represents the deformation contribution, both evaluated in the previous sections. The rocking component can be expressed by θh. By assuming small displacements, the displacements can be written as:

$$u_B - u_D - \delta = \theta h \tag{6}$$

$$v_C = \theta(l - x) \tag{7}$$

Eq. 6 then permits the direct evaluation of the rocking component, which is plotted in Fig. 8(b). By inserting the estimated value of the rotation angle θ in Eq. 7 it is possible to obtain the position of the neutral axis x, which is plotted in Fig. 8(c).

The main remarks about the r fraction and the rocking behaviour illustrated in Fig. 8 follow:

- The ratios between the rocking component and the total displacement group into beams of hyperbolae, like in Fig. 8(b). The higher is the imposed displacement, the higher is the rock-

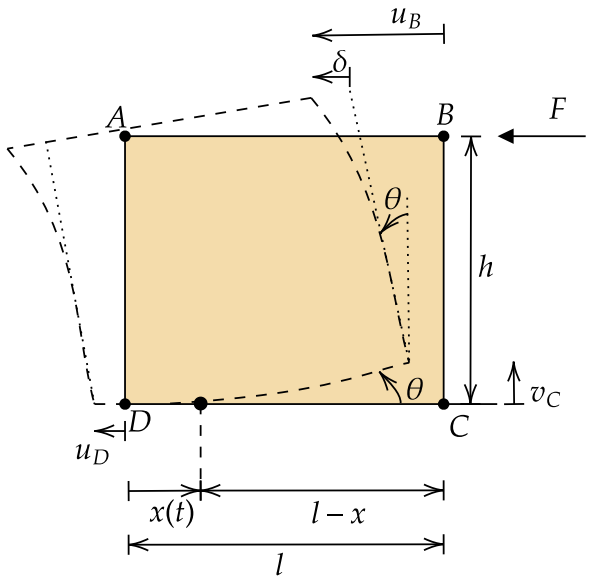

Fig. 7. Displacements field of the wall.

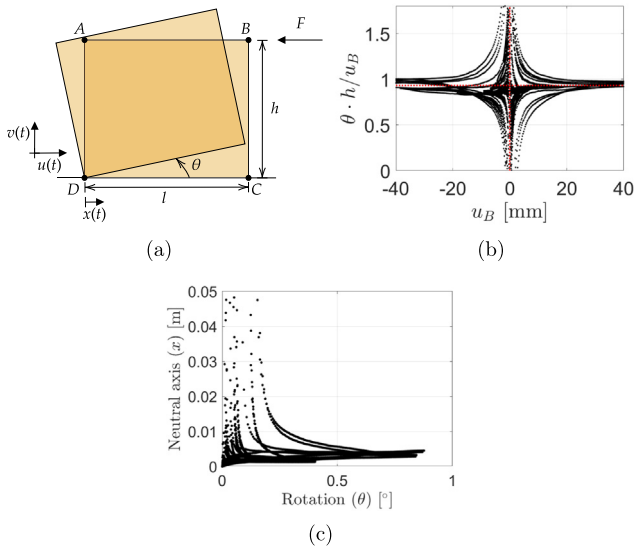

Fig. 8. (a) Illustration of the rigid-body rotation of the panel and the adopted notation; (b) ratio between the displacement in D and B as a function of the imposed displacement according to the loading protocol; (c) Relationship between the neutral axis position and the angle rotation.

ing fraction. Nonetheless, the values corresponding to lower displacements are not entirely reliable: they originate from the division with almost zero values.

- The position of the pivot point x is not zero when the panel rotates: the edges of the panel plasticize and the extension of the compressed area changes. The x value tends to infinity when the panel's rotation approaches zero. When the rotation mounts, the extension of the contact area changes due to plasticization. Fig. 8(c) evidence a sample increment of the contact area as the rotation angle rises. The x value depends on both the rotation angle θ and the past displacement history: the depth of the neutral axis advances as the plasticization raises, given the same rotation angles.
- The horizontal asymptote is a feature of the test configuration, almost independent from the displacement value after a certain load level. The asymptote likely expresses the rocking fraction of the imposed displacement, see Fig. 8(b).

3.4. Rocking, sliding and deformation components: LTF vs CLT

Table 4 reports the three displacement contributions in all the tested specimens, expressed as percentages. The displacement components in Table 4 refer to the post-elastic behaviour. They originate from Eqs. (1),(4),(5) respectively, which present an asymptotic definition of the three displacement fractions. The experimental data reveal that the three displacement components rapidly converge towards a definite value after the elastic phase. The values stationarity proves that the excitation amplitude does not modify the balance between the three contributions after a certain post elastic displacement value.

The prevalent contribution to the total displacement comes from the rigid-body rotation. The rocking motion of LTF shear walls is lower than CLT: LTF shear walls are more deformable than CLT. Table 5 proves and quantifies the diverse in-plane stiffness between the two structural typologies: the first column shows the bending stiffness obtained from the tangent to the first loading curve. In contrast, the second column collects the equivalent elastic modulus obtained by assuming a cantilevered-like behaviour of the panel. The vertical load has almost the same effects in both the shear walls: the load increment reduces the rocking component. The vertical load acts as a rotation restraint. The reduction of the base connections determines a significant increment of the rocking motion, like in the case without hold-downs (WHD). Interestingly the test LTF SCREW, which uses screws distributed uniformly on the bottom rail as a sliding restraint, shows that the presence of screws may influence the rocking mechanism, by offering an additional uplift restraint, thus limiting the rocking percentage as seen from Table 4.

The sliding component does not significantly change between LTF and CLT shear walls. The rigid-body translation mainly depends on the transverse resistance of the base connections and does not likely depend on the vertical load. This shred of information conveys some details about the occurring of friction phenomena. The amount of the Coulomb-type friction restraint depends on the vertical load: the substantial independence of the sliding fraction on the vertical load proves the possible independence of friction in the sliding restraints, primarily provided by the base

Table 4
The table attempts to synthesize the displacement components due to sliding, deformation and rocking, expressed as a fraction of the imposed displacement in point B, estimated using Eqs. (1),(4),(5) respectively.

Test	Sliding-s [%]	Deformation-d [%]	Rocking-r [%]
LTF STD-L0	9.5	4.7	85.9
LTF STD-L10	2.1	17.8	80.1
LTF STD-L20	5.1	21.7	73.2
LTF 2F-L20	3.8	33.4	62.8
LTF 150-L20	7.6	34.6	57.8
LTF 50/RG-L20	7.7	18.8	73.5
LTF 50-L20	0.8	15.4	83.9
LTF SCREW L20	2.0	34.5	63.5
LTF WHD-L10	1.4	8.1	90.5
CLT STD-L0	5.6	4.2	90.2
CLT STD-L20	5.0	12.8	82.3
CLT NA620-L0	7.7	3.8	88.5
CLT NA620-L20	3.6	7.9	88.6
CLT ND620-L0	4.0	8.6	87.4
CLT ND620-L20	8.5	5.7	85.8
CLT NA340-L20	4.1	2.2	93.7
CLT NAWH-L20	6.8	0.1	93.0

Table 5
Estimate of the initial stiffness of the LTF and CLT shear walls and the equivalent elastic modulus.

Test	Bending stiffness [kN/mm]	Equivalent E [MPa]
LTF STD-L0	7.6	337.3
LTF STD-L10	4.1	180.9
LTF STD-L20	10.6	469.8
LTF 2F-L20	10.8	481.8
LTF 150-L20	9.4	419.1
LTF 50/RG-L20	9.4	416.9
LTF 50-L20	6.5	288.9
LTF SCREW L20	20.4	906.2
LTF WHD-L10	7.7	341.3
CLT STD-L0	12.6	561.3
CLT STD-L20	19.6	870.7
CLT NA620-L0	12.2	542.4
CLT NA620-L20	15.4	685.3
CLT ND620-L0	12.4	552.0
CLT ND620-L20	19.6	871.6
CLT NA340-L20	17.5	779.6
CLT NAWH-L20	13.0	576.4

connections. In the current setup, friction phenomena are then negligible compared to the restraining capacity of the connections.

Additionally, Table 4 proves the substantial independence of the sliding component on the angle brackets. The CLT shear wall has four angle brackets, while the LTF shear wall has two. Nonetheless, the CLT sliding is lower than LTF. The sliding fractions are quite similar between the two structural typologies and the increment in the number of the angle brackets does not enhance the sliding restraint, likely.

The panel deformation changes between LTF and CLT as expected. The impact of deformation on shear walls with low load values and a few base connections (WHD) is shallow and very similar between the two structural typologies. However, as the load increases as well as the base connections, the impact of deformation increases in LTF, while CLT does not deform significantly.

Table 4 stores critical information, which may feed copious comments and research considerations. However, the authors preferred to lighten the presentation by reporting four pie charts in Fig. 9, which compare the average contributions in the post-elastic phase shown in Table 4 and the contributions in the elastic phase, estimated by [35] via analytical investigations. In conclusion, the rocking fraction is dominant in all structural typologies and increases compared to elastic behaviour. The sliding fraction does not change significantly between CLT and LTF shear walls and between elastic and post-elastic behaviours. The deformation fraction is predominant in LTF shear walls. Still, it tends to reduce between elastic and post-elastic in both structural typologies, due to the predominance of rocking, i.e. the deformation of the hold-downs.

4. Discussion: the effect of timber plasticization to force redistribution

The dominance of the rocking response due to the hold-downs deformation may inspire the proposal of an elementary capacity model based on the sole hold down reactions. However, the accuracy of the model mostly depends on an accurate estimation of the extension of the compressed area. In contrast with the elastic behaviour, the extension of the compressed area tends towards a sort of plastic asymptote due to the stress redistribution. The definition of the neutral axis is the following:

$$x_p := \lim_{u_B \to \infty} \left| l - \frac{v_C}{\theta} \right| \tag{8}$$

Fig. 10 shows a qualitative evolution of the neutral axis as the base moment increases and the vertical stress redistribute. There are no studies about the trend of the stress in the compressed area, which depends on several factors: e.g. the planarity of contact areas, timber grading and the slenderness of the panel.

Table 6 attests that the extension of the compressed area depends on the vertical load, the in-plane stiffness of the panel and the boundary restraints. The compressed area expands significantly when the vertical load raises, the in-plane stiffness reduces, and there are fewer base connections. An analytical correlation between the x_p variable and the three mentioned variables (vertical load, in-plane stiffness and boundary conditions) is critical for a conservative estimation of forces acting on the base connections. Specifically, the estimation of the pivot point is essential when assessing the force on the hold-downs: the assumption of the pivot point by one edge of the panel would significantly underestimate the hold-down reactions. Table 6 lists the expected extension of the compressed area. The second column presents the percentage ratio between the estimated x_p value and the base length l. The x_p extension depends on the balance between deformation and rocking components: the increment of the deformation fraction yields an increment of the x_p value. In this paper, the authors do not investigate the compressed area extension based on mechanical analytical models. This step would entail dedicated research

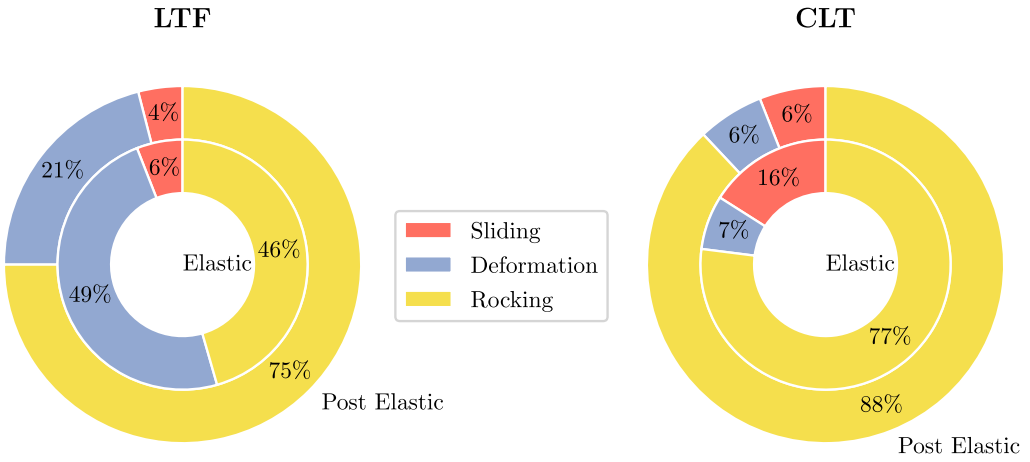

Fig. 9. Percentage of displacement on top of the shear walls due to each single contribution in both the elastic (calculated by [35]) and post-elastic range (as calculated from the experimental data. in this paper).

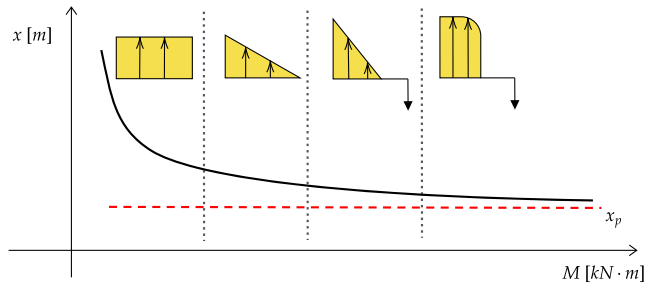

Fig. 10. Qualitative evolution of the neutral axis as a function of the base moment.

Table 6
Estimate of the asymptotic neutral axis in the considered test configurations.

Test	x_p [m]	x_p/l [%]	Rocking-r [%]
LTF STD-L0	0.01	0.4	85.9
LTF STD-L10	0.43	17.2	80.1
LTF STD-L20	0.71	28.2	73.2
LTF 2F-L20	0.72	28.8	62.8
LTF 150-L20	0.02	0.8	57.8
LTF 50/RG-L20	0.01	0.4	73.5
LTF 50-L20	0.01	0.4	83.9
LTF SCREW L20	0.59	23.7	63.5
LTF WHD-L10	0.09	3.6	90.5
CLT STD-L0	0.19	7.5	90.2
CLT STD-L20	0.88	35.4	82.3
CLT NA620-L0	0.20	8.0	88.5
CLT NA620-L20	0.13	5.3	88.6
CLT ND620-L0	0.05	2.0	87.4
CLT ND620-L20	0.70	27.9	85.8
CLT NA340-L20	0.37	14.9	93.7
CLT NAWH-L20	0.48	19.2	93.0

efforts based on adequate mechanical models of the shear wall post-elastic response.

5. Capacity models for timber shear walls

The scientific literature presents several models for assessing the strength of CLT and LTF timber shear walls. The capacity models of LTF walls, like the ones by Källsner and Girhammar [43,44], focus on the role of the sheathing-to-framing connections, by evaluating the resistance of the wall related to that sort of failure. That is also the base for the prediction models present in the current Eurocode 5 proposal. Conversely, many scholars consider CLT walls as rigid bodies: the capacity of the wall depends on the strength of its anchorage system, due to its intrinsic considerable in-plane strength and stiffness[45]. The CLT capacity models merely descend from the equilibrium equations of the wall, while the main differences between them lie on two main points: the inclusion or not of the angle brackets contribution in the tension resisting mechanism, and the shape and contribution of the compression zone. Casagrande [35] and Tomasi [46] both neglect the contribution of angle brackets: the first does not make any specific assumptions about the compression stresses distribution and proposes a conventional lever arm equals to 0.9*l*, the second assumes a rectangular stress block distribution in the compression zone, with size 0.8*x*. Wallner-Novak [47] proposes a model similar to [46] but with compression zone equals to 0.25*l*. Pei [48], Reynolds [49], Gavric [50] presented models that include the tensile contribution of angle brackets. Pei [48] assumes an elastic triangular distribution of tensile forces, by considering the rigid body rotation around one edge of the shear wall. Reynolds [49] presented three different models, which all include the presence of a compression zone, but differ in the size of that zone and the distribution of tensile forces between angle brackets and hold-down. Gavric [50] presents a model similar to [48], but considers the interaction between horizontal and vertical forces on the angle brackets.

The simplified capacity model presented in this paper, based on equilibrium equations, is the same in both LTF and CLT walls. As evidenced by the experimental campaign and the previous sections, the behaviour of LTF walls is mainly governed by the hold-down connections. As shown in Fig. 11, the wall is assumed to pivot around the position *P* of its neutral axis, characterized by a compression region of extension x_p; no specific assumption is made regarding the shape of the stress distribution in the compression zone. The contribution of angle brackets to the racking mechanism is neglected. Hereafter follows the equilibrium equations:

$$\uparrow \quad -q \cdot l - H + k_C \sigma_C \cdot x_p \cdot t_{\text{eff}} = 0 \tag{9}$$

$$F \cdot h - q \cdot l \cdot \left(\frac{l}{2} - x_p\right) - H \cdot (l - x_p) + k_C \sigma_C \cdot x_p \cdot t_{\text{eff}} \cdot l_c = 0 \tag{10}$$

where q is the distributed vertical load, l the wall length, F the top horizontal force, h the wall height, H the hold down reaction force, σ_c the averaged compression stress on timber, k_c a modification parameter which accounts for the increment of resistance due to compression hardening and the shape feature of the stress diagram, x_p the extension of the neutral axis, t_{eff} is the thickness of the wall reacting in compression, l_c is the lever arm of the compression region. The k_c and the l_c factors are in fact unknown. The goal of this section is to demonstrate that the cyclic behaviour of the tested shear walls is mainly dependent on the hold-down. The force acting on the wall is then evaluated by considering the sole hold-down contribution to the rotational equilibrium, and neglecting the contribution of the unknown compression stresses in timber:

$$F = H \cdot \frac{\tau \cdot l}{h} + q \cdot \frac{l}{h}\left(\tau \cdot l - \frac{l}{2}\right) \quad | \quad \tau = \frac{l - x_p}{l} \tag{11}$$

Eq. 11 bestows the top horizontal force acting on the wall, given the hold-down force *H*, the vertical load *q* and the position of the pivot point x_p. The authors validated this model by comparing, in

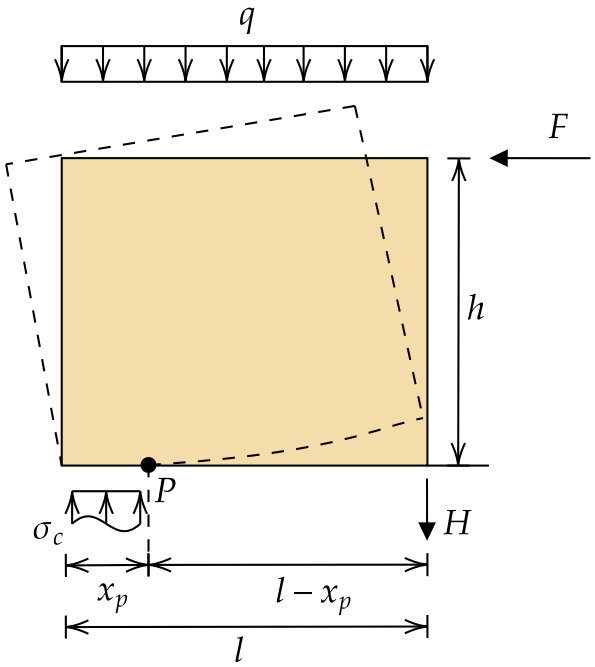

Fig. 11. Mechanical model of the shear wall.

terms of cyclic curves and maximum force values, the forces measured in point B of the shear wall, with the horizontal force $F(t)$. $F(t)$ is obtained from the simplified model in Eq. 11, using the forces measured on the hold-downs $H(t)$ and the pivot point x_p value estimated in Table 6.

Figs. 12,13 show the two comparing curves: the dotted red curve is the simplified model in Eq. 11, while the solid black one is the force measured in B. Accurately, the dotted red curves Figs. 12,13 derive from plugging the hold down reaction H measured during the experimental test into Eq. 11. The positive and negative reaction values originate from the sense of rotation: if the panel rotates anticlockwise, the authors used the force values measured by the right hold-down with a positive sign. If the panel rotates clockwise, the left hold-down reaction is used with a negative sign. Consequently, the top force values are positive or negative depending on the sense of rotation and the particular hold-down subjected to tension loading, see Fig. 11. The visual inspection of the pictures suggests an optimal matching. Table 7 quantifies the discrepancies between the two curves in terms of the maximum forces.

The agreement between the two curves may be considered entirely satisfactory, given the roughness of the model and the numerous restrictions. The presented capacity model grasps the maximum forces attained by the experimental curves. Conversely, the model fails in following the loading and unloading paths closely. The experimental curves exhibit a more gradual force increment/reduction compared to the dotted lines. This difference likely depends on the lack of the angle brackets contribution, which offer a definite resistance in both the loading and unloading phases, and the contribution of the compression stresses in timber. The percentage error is below 10% in the worst cases. Table 7 proves that a capacity model based on the sole hold down reaction is quite faithful, and an elementary formula for the prediction of the hold-down response could descend by taking the 95% percentile of a Gaussian distribution of the τ factor in Eq. 11. Accurately, the 95% percentiles of the τ factor in the LTF and CLT shear walls are:

$$\begin{aligned} \tau_{\mathrm{LTF},95\%} &= 0.81 \\ \tau_{\mathrm{CLT},95\%} &= 0.86 \end{aligned} \tag{12}$$

These values suggest that the estimate of F needs a proper reduction of the pivot point of the hold-downs. The decrease is higher in the case of LTF shear walls due to the higher deformability. Eqs. 11,12 represent simplified formulations possibly useful for engineering purposes, which attempts to avoid underestimating the hold-down reaction by reducing the distance of the rotation point. In conclusion, LTF and CLT shear walls do not display significant differences in the considered configurations. This fact is essentially due to the overstrength of the panel to the base resistance derived from the base connections. Fig. 14 illustrates the probability distributions of two resisting mechanisms: the failure reached during testing, mainly due to hold-down collapse, and the OSB sheathing/CLT panel collapse. The experimental probability density functions of the CLT and LTF shear walls are calculated directly from the values of failure of the cyclic tests. The probability density functions related to the capacity of the CLT panel/ OSB sheathings derive by assuming the same variance of the corresponding experimental curves, and by assuming the shear failure of the OSB sheathing in LTF walls and the in-plane torsional shear

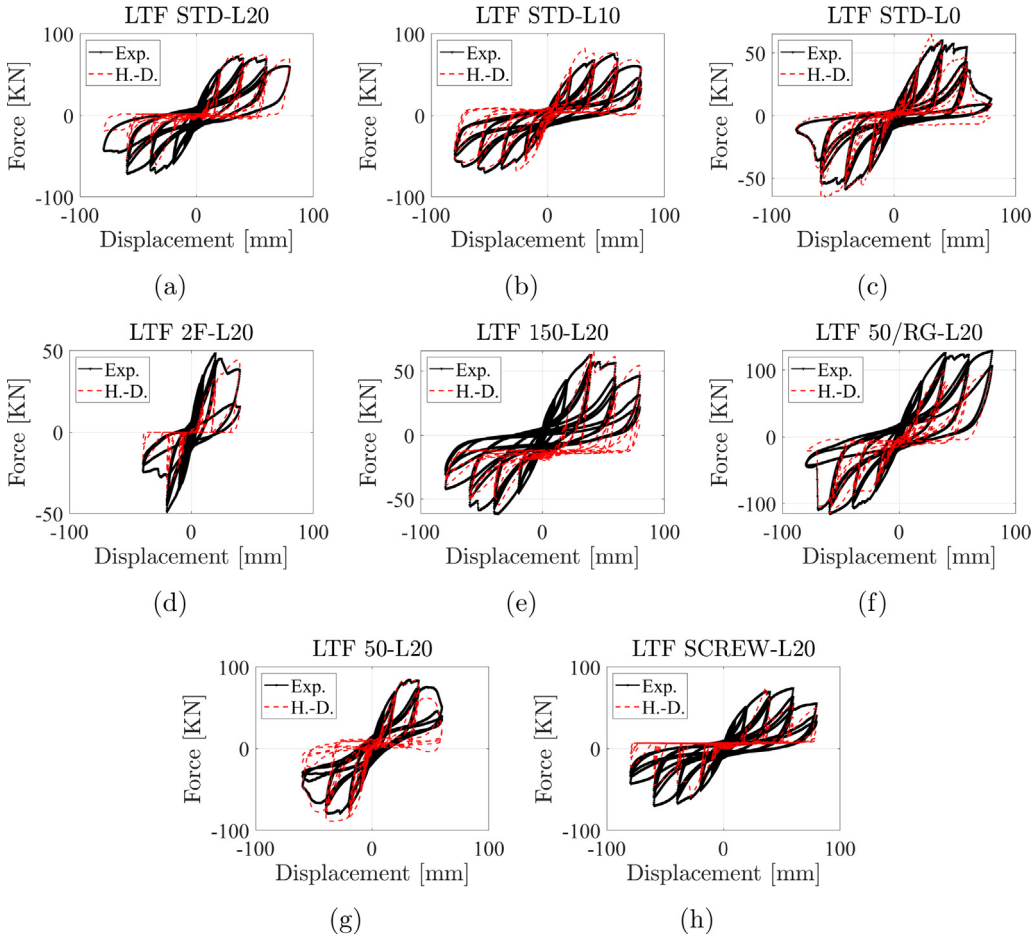

Fig. 12. Comparison between the experimental cyclic response of LTF shear walls and the capacity model based on hold-down measured forces.

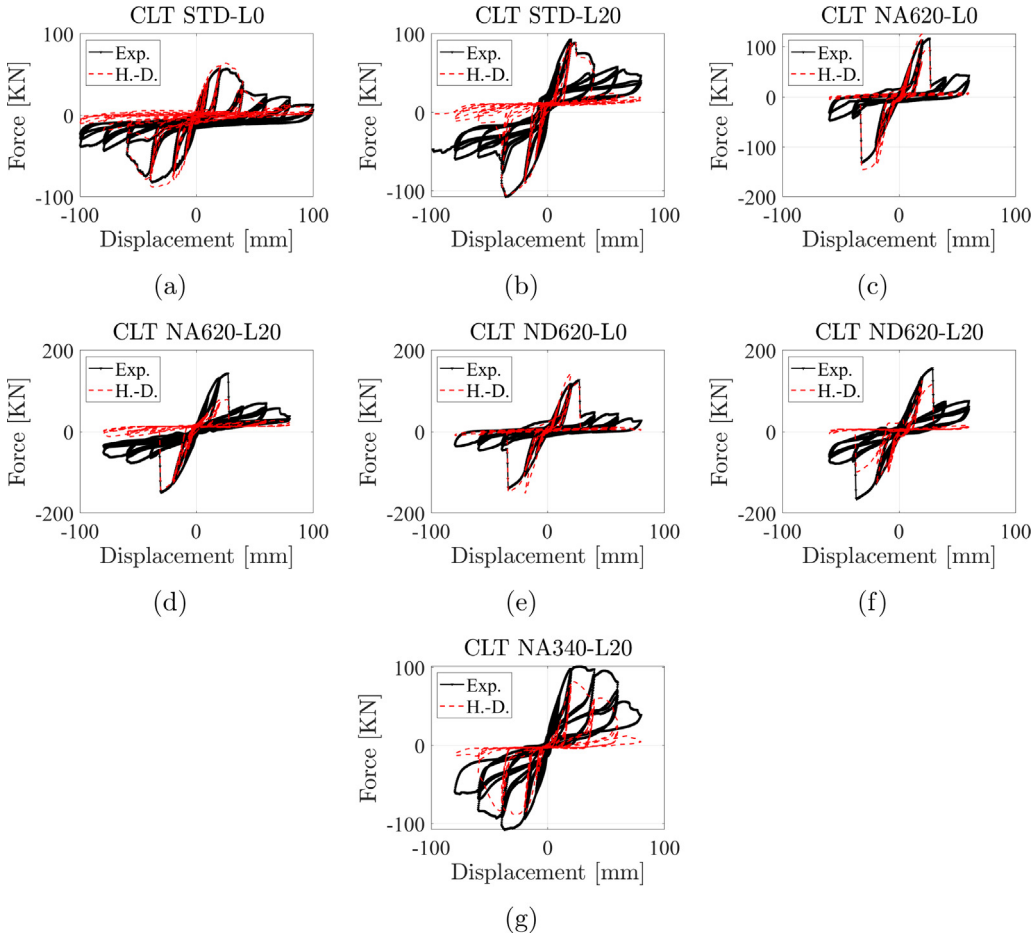

Fig. 13. Comparison between the experimental cyclic response of CLT shear walls and the capacity model based on hold-down measured forces.

Table 7
Comparison between the maximum forces attained by the experimental cyclic tests and the capacity model based on the sole hold-down reactions.

Test	Experimental data	Analytical model	
	F_{max} [kN]	F_{max} [kN]	Error [%]
LTF STD-L0	72.8	75.9	−4.3
LTF STD-L10	75.6	82.7	−9.3
LTF STD-L20	75.6	68.1	10.0
LTF 2F-L20	60.0	54.6	9.0
LTF 150-L20	62.7	65.9	−5.2
LTF 50/RG-L20	128.9	116.1	9.9
LTF 50-L20	84.4	89.0	−5.4
LTF SCREW L20	74.2	74.7	−0.6
		$Avg\,\lvert Error\rvert$	6.7
CLT STD-L0	81.3	87.9	−8.1
CLT STD-L20	107.6	105.5	1.9
CLT NA620-L0	131.1	144.9	−10.5
CLT NA620-L20	143.6	149.5	−4.2
CLT ND620-L0	138.8	151.6	−9.2
CLT NDS20-L20	165.2	148.7	10.0
CLT NA340-L20	107.5	98.4	8.5
		$Avg\,\lvert Error\rvert$	7.5

failure in CLT panels (see [51,52]). The authors used the following values of strength: $f_{vk} = 6.8$ MPa for OSB/3 and $f_{v,\mathrm{tor},k} = 2.5$ MPa for CLT [53,54]. Fig. 14 expresses the true nature of the considered structural systems. The two systems behave likewise due to the similarity of the base connections. Still, the CLT panel is far more resistant than the LTF when different boundary restraints and loads may activate other resisting mechanisms.

$$\gamma_{RD} = \frac{R_{k,b}}{R_{k,d}} \tag{13}$$

The authors reported the overstrength values, estimated as shown in Eq. 13. $R_{k,b}$ is the characteristic load bearing capacity of the panel assuming the timber failure mode (brittle), while $R_{k,d}$ the characteristic load bearing capacity of the panel assuming

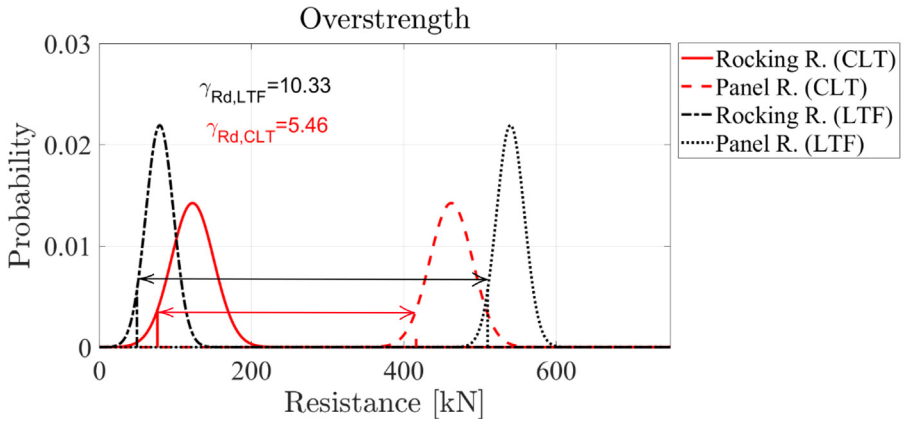

Fig. 14. Comparison between the experimental cyclic response of CLT shear walls and the capacity model based on Hold-Down measured forces.

the hold-down failure mode (ductile). The characteristic values are set equal to the 5-th percentile of the corresponding strength distributions. In the considered cases, the overstrength of LTF shear walls is almost two times of that of CLT. The obtained overstrength values are not general and depend from the specific structural configurations and the considered failure modes. The extension of these results to different structural arrangements must be the object of devoted efforts by the authors.

6. Concluding remarks

Light Timber Frame (LTF) and Cross Laminated Timber (CLT) shear walls exhibit similar response under cyclic loading. The authors compared the experimental test of LTF and CLT wall assemblies characterised by similar geometric features. The first part of the paper describes the test results on nine LTF and eight CLT specimens. Then, the multi-channels force and displacement acquisitions are used to extract three deformation contributions from the shear walls lateral displacement in the post-elastic range: the rigid-body translation (sliding) and rotation (rocking), and the panel deformation (which includes all the contribution not included in the previous ones, such as sheathing-to-framing deformation for LTF and OSB/CLT in-plane shear deformation). The rigid-body rotation is the predominant contribution. This contribution, expressed in percentage to the total deformation, is on average 75% and 88% in LTF and CLT specimens, respectively. The rocking response dominance, due to the hold-down deformation contribution, inspired an elementary capacity model based on the hold down reactions and the assumption of a pivot point. The 95^{th} percentile of the Gaussian probability distribution of the ratio between the extension of the compressed area and the panel length is about 0.2: the adoption of the panel edge as a rotation point would determine an approximate 20% underestimation of the hold down reactions in the considered capacity model.

The simplified capacity model based on the measured hold-down reactions and the estimated pivot point led to an excellent agreement with the experimental lateral response. The error in term of the maximum force attained during the cycles is less than 10%. The two systems, LTF and CLT, behave likewise due to the similarity of the base connections. This fact is essentially due to the wall assembly overstrength to the resistance of the base connections. The overstrength ratios between the CLT panel/OSB sheathing and the panel resistance due to the hold down collapse are approximately 5.46 and 10.33 for the CLT and LTF shear walls respectively. The overstrength ratio features the intrinsic difference between the two structural systems, although the hold-down failure mode conceals such diversity. The authors will aim at assessing the approximation related to more accurate capacity model and will endeavour to determine the shape of the stress distribution of the compressed area. The estimation of the stress distribution would yield the estimate of the shape factor of an equivalent rectangular stress-block. The assessment of the compressed timber resisting contribution would drive mindful reinforcement methods for compression perpendicular to grain in top/bottom plates of Light Timber Frames, like in [55].

CRediT authorship contribution statement

Angelo Aloisio: Conceptualization, Methodology, Software, Data curation, Writing - review & editing. **Francesco Boggian:** Conceptualization, Methodology, Writing - review & editing. **Roberto Tomasi:** Supervision. **Massimo Fragiacomo:** Supervision.

Declaration of Competing Interest

The authors declare that they have no known competing financial interests or personal relationships that could have appeared to influence the work reported in this paper.

Acknowledgements

The authors acknowledge the research efforts of Paolo Grossi, Paolo Endrizzi, Tiziano Sartori and Ermanno Acler, who carried out the experimental tests with the support of the staff of the University of Trento.

References

[1] A. Aloisio, M. Fragiacomo, G. D'Alò, Traditional tf masonries in the city centre of l'aquila–the baraccato aquilano, Int. J. Architectural Heritage (2019) 1–18.
[2] A. Aloisio, M. Fragiacomo, G. D'Alò, The 18th-century baraccato of l'aquila, Int. J. Architectural Heritage (2019) 1–15.
[3] S. Thelandersson, H.J. Larsen, Timber engineering, John Wiley & Sons, 2003.
[4] M. Piazza, R. Tomasi, and R. Modena, Strutture in legno, Materiale, calcolo e progetto secondo le nuove normative europee (Wooden structures. Material, calculation and design according to the new European regulations). Biblioteca Tecnica Hoepli Milano, Milano, 2005, pp. 512–558..
[5] A. Aloisio, D. Pasca, R. Tomasi, M. Fragiacomo, Dynamic identification and model updating of an eight-storey clt building, Eng. Struct. 213 (2020) 110593.
[6] V.A. De Araujo, J. Cortez-Barbosa, J.N. Garcia, M. Gava, C. Laroca, S.F. César, Woodframe: light framing houses for developing countries, J. Constr. 15 (2) (2020) 78–87.
[7] I. Gavric, M. Fragiacomo, A. Ceccotti, Cyclic behavior of clt wall systems: experimental tests and analytical prediction models, J. Struct. Eng. 141 (11) (2015) 04015034.
[8] D. Casagrande, S. Rossi, R. Tomasi, G. Mischi, A predictive analytical model for the elasto-plastic behaviour of a light timber-frame shear-wall, Constr. Build. Mater. 102 (2016) 1113–1126.
[9] A. Aloisio, R. Alaggio, M. Fragiacomo, Fragility functions and behavior factors estimation of multi-story cross-laminated timber structures characterized by

an energy-dependent hysteretic model, Earthquake Spectra (2020). 8755293020936696.
[10] A. Hashemi, P. Zarnani, P. Quenneville, Seismic assessment of rocking timber walls with energy dissipation devices, Eng. Struct. 221 (2020) 111053.
[11] D. Fitzgerald, T.H. Miller, A. Sinha, J.A. Nairn, Cross-laminated timber rocking walls with slip-friction connections, Eng. Struct. 220 (2020) 110973.
[12] G. Poh'Sie, C. Chisari, G. Rinaldin, C. Amadio, M. Fragiacomo, Optimal design of tuned mass dampers for a multi-storey cross laminated timber building against seismic loads, Earthquake Eng. Struct. Dyn. 45 (12) (2016) 1977–1995.
[13] M. Koliou, A. Filiatrault, Development of wood and steel diaphragm hysteretic connector database for performance-based earthquake engineering, Bull. Earthq. Eng. 15 (10) (2017) 4319–4347.
[14] Z. Chen, M. Popovski, A. Iqbal, Structural performance of post-tensioned clt shear walls with energy dissipators, J. Struct. Eng. 146 (4) (2020) 04020035.
[15] Y. Cui, Z. Shu, R. Zhou, Z. Li, F. Chen, Z. Ma, "Self-centering steel–timber hybrid shear wall with slip friction dampers: Theoretical analysis and experimental investigation, The Structural Design of Tall and Special Buildings, 2020, p. e1789..
[16] A. Aloisio, R. Alaggio, J. Köhler, M. Fragiacomo, Extension of generalized bouc-wen hysteresis modeling of wood joints and structural systems, J. Eng. Mech. 146 (3) (2020) 04020001.
[17] A.J. Salenikovich, The racking performance of light-frame shear walls (Ph.D thesis), Virginia Tech, 2000..
[18] J.P. Judd, F.S. Fonseca, Analytical model for sheathing-to-framing connections in wood shear walls and diaphragms, J. Struct. Eng. 131 (2) (2005) 345–352.
[19] R. Tomasi, T. Sartori, Mechanical behaviour of connections between wood framed shear walls and foundations under monotonic and cyclic load, Constr. Build. Mater. 44 (2013) 682–690.
[20] A. Iqbal, M. Fragiacomo, S. Pampanin, A. Buchanan, Seismic resilience of plywood-coupled lvl wall panels, Eng. Struct. 167 (2018) 750–759.
[21] D. Way, A. Sinha, F.A. Kamke, Performance of light-frame timber shear walls produced with weathered sheathing, J. Architectural Eng. 26 (1) (2020) 04019022.
[22] F. Alinoori, P. Sharafi, F. Moshiri, B. Samali, Experimental investigation on load bearing capacity of full scaled light timber framed wall for mid-rise buildings, Constr. Build. Mater. 231 (2020) 117069.
[23] T.T. Nguyen, T.N. Dao, S. Aaleti, J.W. van de Lindt, K.J. Fridley, Seismic assessment of a three-story wood building with an integrated clt-lightframe system using rths, Eng. Struct. 167 (2018) 695–704.
[24] R.L. Tuomi, W.J. McCutcheon, Racking strength of light-frame nailed walls, J. Struct. Div. 104 (7) (1978) 1131–1140.
[25] A.K. Gupta, G.P. Kuo, Behavior of wood-framed shear walls, J. Struct. Eng. 111 (8) (1985) 1722–1733.
[26] J. Dolan, R. Foschi, Structural analysis model for static loads on timber shear walls, J. Struct. Eng. 117 (3) (1991) 851–861.
[27] G. Rinaldin, C. Amadio, M. Fragiacomo, A component approach for the hysteretic behaviour of connections in cross-laminated wooden structures, Earthquake Eng. Struct. Dyn. 42 (13) (2013) 2023–2042.
[28] P. Grossi, T. Sartori, I. Giongo, R. Tomasi, Analysis of timber log-house construction system via experimental testing and analytical modelling, Constr. Build. Mater. 102 (2016) 1127–1144.
[29] M. Koliou, J.W. van de Lindt, R.O. Hamburger, Nonlinear modeling of wood-frame shear wall systems for performance-based earthquake engineering: Recommendations for the asce 41 standard, J. Struct. Eng. 144 (8) (2018) 04018095.
[30] G.C. Foliente, Hysteresis modeling of wood joints and structural systems, J. Struct. Eng. 121 (6) (1995) 1013–1022.
[31] A. Kottari, A. Charalampakis, V. Koumousis, A consistent degrading bouc–wen model, Eng. Struct. 60 (2014) 235–240.
[32] J. Song, A. Der Kiureghian, Generalized bouc–wen model for highly asymmetric hysteresis, J. Eng. Mech. 132 (6) (2006) 610–618.
[33] S. Sessa, N. Vaiana, M. Paradiso, L. Rosati, An inverse identification strategy for the mechanical parameters of a phenomenological hysteretic constitutive model, Mech. Syst. Signal Process. 139 (2020) 106622.
[34] G. Di Gangi, C. Demartino, G. Quaranta, G. Monti, Dissipation in sheathing-to-framing connections of light-frame timber shear walls under seismic loads, Eng. Struct. 208 (2020) 110246.
[35] D. Casagrande, S. Rossi, T. Sartori, R. Tomasi, Proposal of an analytical procedure and a simplified numerical model for elastic response of single-storey timber shear-walls, Constr. Build. Mater. 102 (2016) 1101–1112.
[36] P. Grossi, T. Sartori, R. Tomasi, Tests on timber frame walls under in-plane forces: part 2, Proc. Inst. Civil Eng.-Struct. Build. 168(11) (2015) 840–852..
[37] E. Acler, R. Tomasi, Monotonic and cyclic in-plane behavior of clt panels tested by using different types of metal devices, in COST Action FP1004 – Early Stage Researchers Conference Enhance mechanical properties of timber, engineered wood products and timber structures – Zagreb, Croatia, 2012..
[38] R. Tomasi, Seismic behavior of connections for buildings in clt, in COST Action FP1004 – Focus Solid Timber Solutions European Conference on Cross Laminated Timber (CLT) – Graz, Austria, 2013.
[39] M. Andreolli, R. Tomasi, Bemessung von gebäuden in brettsperrholzbauweise unter erdbebenbeanspruchung, Bautechnik (2016).
[40] P. Grossi, PARETI INTELAIATE IN LEGNO: indagine sul comportamento meccanico tramite prove sperimentali a scala reale (Master's thesis), University of Trento, 2011..
[41] P. Endrizzi, I sistemi di connessione di base del pannello xlam compensato di tavole indagine sperimentale in scala reale e modellazione numerica della capacità portante globale di parete ottenuta con l'impiego di una nuova tipologia di angolare a taglio Master's thesis, University of Trento, 2011.
[42] EN 594:2011 Timber structures, Test methods – Racking strength and stiffness of timber frame wall panels, BSI, London UK, 2011..
[43] B. Källsner, U. Girhammar, Analysis of fully anchored light-frame timber shear walls-elastic model, Mater. Struct./Materiaux et Constructions 42 (3) (2009) 301–320.
[44] B. Källsner, U. Girhammar, Plastic models for analysis of fully anchored light-frame timber shear walls, Eng. Struct. 31 (9) (2009) 2171–2181.
[45] I. Lukacs, A. Björnfot, R. Tomasi, Strength and stiffness of cross-laminated timber (clt) shear walls: State-of-the-art of analytical approaches, Eng. Struct. 178 (2019) 136–147.
[46] S. Pei, J. Lindt, M. Popovski, Enhance mechanical properties of timber, engineered wood products and timber structures, CLT course at FPS COST Action FP1004. CLT Training School, 2014..
[47] M. Wallner-Novak, J. Koppelhuber, K. Pock, Brettsperrholz Bemessung Grundlagen für Statik und Konstruktion nach Eurocode, proHolz Austria (2013).
[48] S. Pei, J. Lindt, M. Popovski, Approximate r-factor for cross-laminated timber walls in multistory buildings, J. Architectural Eng. 19 (2013) 245–255.
[49] T. Reynolds, R.M. Foster, J. Bregulla, W. Shao Chang, R. Harris, M. Ramage, Lateral load resistance of cross-laminated timber shear walls, J. Struct. Eng.-ASCE 143 (2017) 06017006..
[50] I. Gavric, M. Popovski, Design models for clt shearwalls and assemblies based on connection properties, in: Proceedings of International Network on Timber Engineering Research INTER/47-15-4, 2014.
[51] D. Casagrande, T. Sartori, R. Tomasi, Capacity design approach for multi-storey timber-frame buildings, in: Proceedings of International Network on Timber Engineering Research INTER/47-15-3, 2014.
[52] F. Boggian, M. Andreolli, R. Tomasi, Cross laminated timber (clt) beams loaded in plane: testing stiffness and shear strength, Front. Built Environ. 5 (2019) 58.
[53] EN 300:2006, Oriented strand boards (OSB). Definitions, classification and specifications, 2006..
[54] R. Brandner, G. Flatscher, A. Ringhofer, G. Schickhofer, A. Thiel, Cross laminated timber (clt): overview and development, Eur. J. Wood Wood Products 74 (3) (2016) 331–351.
[55] F. Alinoori, F. Moshiri, P. Sharafi, B. Samali, Reinforcement methods for compression perpendicular to grain in top/bottom plates of light timber frames, Constr. Build. Mater. 231 (2020) 116377.